Fault-tolerant control on three-tank system using fuzzy brain emotional learning controller

Pham Duc Hung[1], **Phan Anh Tuan**[2], **Do Van Tan**[3] **and Bui The Thanh**[4,*]

[1]*Faculty of Electrical and Electronic Engineering, Hung Yen University of Technology and Engineering, Hung Yen, Vietnam*
[2]*Control Automation in Production and Improvement of Technology Institute (CAPITI), 89 Ly Nam De, Ha Noi, Vietnam*
[3]*Faculty of Technology and Engineering, Hai Phong University, Hai Phong, Vietnam*
[4]*Faculty of Mechanical and Electrical Engineering, Hanoi Industrial and Trade University, Ha Noi, Vietnam*
[*]*Corresponding author E-mail: thanhbt@hict.edu.vn*
DOI: https://doi.org/10.64032/mca.v30i4.450

Abstract

This paper develops a fault-tolerant control scheme for a nonlinear, hydraulically coupled three-tank process subject to abrupt and incipient leakage faults. The architecture combines a nominal sliding-mode controller (SMC) with a fuzzy brain emotional learning controller (FBELC) that learns the lumped fault-induced dynamics and model uncertainty online. A systematic flow-balance model, an actuator-aware command path, and a Lyapunov analysis are provided to establish boundedness and uniform ultimate boundedness of the closed-loop signals. Four simulation scenarios cover uncontrolled, fault-free controlled, single abrupt-fault, and simultaneous abrupt/incipient-fault operation. In the most demanding simultaneous-fault case, the proposed method yields RMSE values of 0.0263, 0.0121, and 0.0149 m for Tanks 1–3, respectively, with an average RMSE of 0.0178 m. This represents reductions of 27.6% relative to CMAC (0.0246 m) and 15.6% relative to FCMAC (0.0211 m), demonstrating improved liquid-level tracking and fault accommodation while retaining a compact online-learning structure suitable for real-time implementation.

Keywords: *Brain Emotional Learning Controller; Fault-Tolerant Control; Fuzzy System; Level Tank System*

Symbols

Symbols	Units	Description
$y_i(k)$	m	Liquid level of the i-th tank
u_i	m^3/s	Control input supplied by the pump
$f_i(k)$	–	Fault function of the tank system
$\beta_i(k-T_i)$	–	Time profile of the fault
$\chi_i(y,u)$	–	System uncertainty of the i-th tank
A, S_p	m^2	Tank cross-section and connection pipe cross-section
g	m/s^2	Gravitational acceleration
$e_i(k)$	m	Tracking error of the i-th tank
u_{iN}, u_{iC}	m^3/s	Nominal and corrective control components

1. Introduction

Fault-tolerant control (FTC) plays an essential role in nonlinear process systems, where unexpected component degradation, uncertain hydraulic parameters, and external disturbances may seriously deteriorate closed-loop performance or even drive the plant to unsafe operating conditions [1], [2], [3], [4], [5], [6], [7], [8]. Among process-control benchmarks, the three-tank system is widely used to evaluate FTC strategies because its dynamics are nonlinear, strongly coupled, and directly affected by inflow/outflow constraints and inter-tank hydraulic interactions [8]. Therefore, maintaining stable liquid levels under abnormal operating conditions is critical for safety, reliability, and continuous operation.

In practical tank systems, faults may appear in several forms, including actuator faults in pumps or valves, leakage faults in tanks or connection pipes, abrupt faults caused by sudden component damage, and incipient faults caused by gradual degradation over time [2], [7], [8]. These faults are difficult to compensate for because their occurrence times, magnitudes, and time profiles are generally unknown. Abrupt faults can generate large transient tracking errors immediately after occurrence, whereas incipient faults are more difficult to detect and compensate for because their effects develop slowly and may be masked by nonlinear dynamics, uncertainties, and disturbances [5], [9], [10], [11].

Various FTC approaches have been developed for uncertain nonlinear systems. Sliding-mode control (SMC) is attractive because of its robustness against matched uncertainties, but it may require conservative switching gains and may suffer from chattering when discontinuous sign functions are used [12], [13], [14]. Fuzzy and neural-network controllers can approximate unknown nonlinear functions, but their online learning performance may degrade when many parameters must be updated simultaneously [15], [16]. CMAC-based and FCMAC-based fault-accommodation controllers provide fast local learning and have been applied to tank systems [7], [8], [16]; however, their approximation performance depends on memory allocation, receptive-field design, and parameter tuning. Brain emotional learning control (BELC) and fuzzy brain emotional learning control (FBELC), inspired by the amygdala and orbitofrontal learning mechanism, offer a compact emotional-learning structure for online compensation and have shown potential for uncertain nonlinear control

Received: 19 June 2026; Revised: 22 September 2026; Accepted: 13 October 2026.

systems [17], [18], [19], [20]. Nevertheless, the integration of SMC and FBELC for three-tank fault accommodation under abrupt and incipient leakage faults still requires a systematic controller design, stability analysis, and quantitative comparison. Recent FTC studies have also treated combined actuator and sensor faults in process systems [21], while recent FBELC designs have emphasized compact adaptive structures for uncertain nonlinear plants [22]. Recent MCA contributions similarly highlight constraint-aware nonlinear and fault-resilient control implementation [23], [24].

Motivated by the above discussion, this paper develops an SMC-FBELC FTC scheme for nonlinear three-tank systems subject to abrupt and incipient leakage faults. The nominal SMC component is used to preserve the desired tracking behavior, whereas the FBELC corrective component estimates and compensates for unknown fault-induced dynamics and system uncertainties online. By combining the robustness of SMC with the adaptive learning ability of FBELC, the proposed scheme aims to improve tracking accuracy and fault-accommodation capability without requiring exact prior knowledge of the fault functions.

The main contributions of this paper are summarized as follows:

(1) An FBELC fault-tolerant control architecture is developed for nonlinear three-tank systems under abrupt and incipient leakage faults.
(2) The FBELC corrective controller is designed to approximate unknown fault-induced dynamics and system uncertainties online.
(3) A Lyapunov-based stability analysis is provided to prove boundedness of the closed-loop signals.
(4) Four simulation cases and RMSE comparison with CMAC and FCMAC are presented to verify the tracking and fault-accommodation performance.

The remainder of this paper is organized as follows. Section 2 presents the three-tank system, fault model, control objective, and discrete-time representation. Section 3 introduces the proposed SMC-FBELC fault-tolerant controller. Section 4 provides the Lyapunov-based stability analysis. Section 5 presents simulation results and discussions. Section 6 concludes the paper and outlines future research directions.

2. Problem formulation

2.1 General nonlinear system with faults

Consider the following nonlinear dynamic system affected by unknown faults and uncertainties:

$$\dot{y}(t) = F(y,t) + G(y,t)\left[u(t) + \xi(y,t) + B(t-T)f(y,t)\right]. \tag{1}$$

where $y \in \mathbb{R}^m$ is the state vector, $u(t) \in \mathbb{R}^m$ is the control input, $F(y,t)$ and $G(y,t)$ denote the nominal nonlinear dynamics, $\xi(y,t)$ represents the lumped uncertainty and external disturbance, $f(y,t)$ is an unknown fault function, and T is the fault occurrence time. The matrix $B(t-T)$ describes the time profile of the fault and is written as

$$B(t-T) = \mathrm{diag}\{b_1(t-T), \ldots, b_m(t-T)\}. \tag{2}$$

The functions $b_i(t-T)$ characterize whether the corresponding fault is abrupt, incipient, or inactive. In this paper, both abrupt and incipient leakage faults are considered.

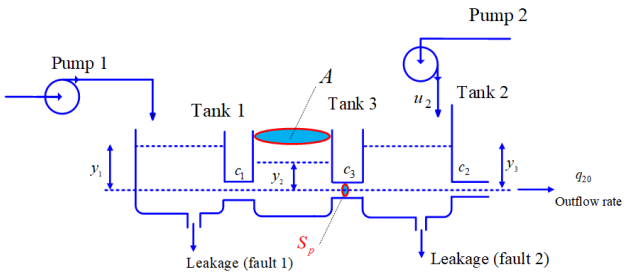


Figure 1. Schematic diagram of the three-tank system with leakage faults.

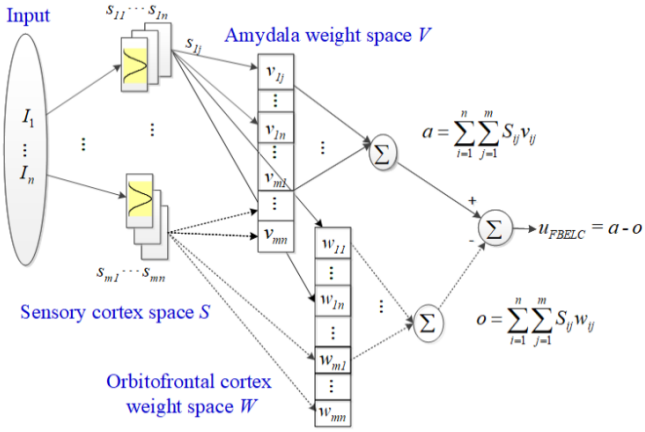


Figure 2. Fuzzy brain emotional learning controller structure.

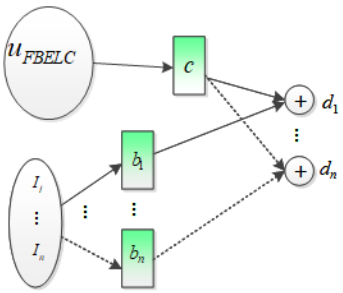


Figure 3. The parameter adjustment algorithm of FBELC.

2.2 Three-tank dynamics and control objective

The continuous-time dynamics of the three-tank system, illustrated in Fig. 1, are described as

$$\dot{y}_1 = \frac{1}{A}\left[-z_1 S_p \,\mathrm{sgn}(y_1 - y_3)\sqrt{2g|y_1 - y_3|} + u_1\right] + \chi_1(y,u), \tag{3a}$$

$$\dot{y}_2 = \frac{1}{A}\left[-z_3 S_p \,\mathrm{sgn}(y_2 - y_3)\sqrt{2g|y_2 - y_3|} - z_2 S_p\sqrt{2gy_2} + u_2\right] + \chi_2(y,u), \tag{3b}$$

$$\dot{y}_3 = \frac{1}{A}\left[z_1 S_p \,\mathrm{sgn}(y_1 - y_3)\sqrt{2g|y_1 - y_3|} - z_3 S_p \,\mathrm{sgn}(y_3 - y_2)\sqrt{2g|y_3 - y_2|}\right] + \chi_3(y,u), \tag{3c}$$

where $y = [y_1, y_2, y_3]^T$, $u = [u_1, u_2]^T$, $g = 9.8$ m/s^2, $A = 0.0154$ m^2, $S_p = 5 \times 10^{-5}$ m^2, and $z_1 = 1$, $z_2 = 0.8$, $z_3 = 1$

are the outflow coefficients.

Physical configuration and signal definitions. The benchmark comprises three open tanks of equal cross-sectional area A. Tank 1 and Tank 2 receive the manipulated pump inflows u_1 and u_2 (m^3/s), respectively; Tank 3 is not directly actuated. Tanks 1–3 are hydraulically coupled through pipes of cross-sectional area S_p. The measured/controlled outputs are the liquid heights $y = [y_1, y_2, y_3]^T$ (m). The outlet from Tank 2 discharges to the reservoir, and leakage ports in Tanks 1 and 2 generate the abrupt and incipient fault flows. The sign functions in (3) permit bidirectional inter-tank flow: flow is positive from the higher level toward the lower level.

Derivation from conservation of volume. For each tank, $A\dot{y}_i$ equals total inflow minus total outflow. Torricelli's law gives $q_{ij} = z_{ij} S_p \operatorname{sgn}(y_i - y_j)\sqrt{2g|y_i - y_j|}$ for an interconnection and $q_{20} = z_2 S_p \sqrt{2g y_2}$ for the outlet. Consequently, $A\dot{y}_1 = u_1 - q_{13} + A\chi_1$, $A\dot{y}_2 = u_2 + q_{32} - q_{20} + A\chi_2$, and $A\dot{y}_3 = q_{13} - q_{32} + A\chi_3$. Dividing these three balance equations by A gives (3a)–(3c). Here χ_i collects parameter mismatch and unmodeled disturbances in level-rate units. The physical domain is $y_i \geq 0$; square-root terms are evaluated only in this domain.

The plant therefore has three states/outputs but only two independent control inputs. Tracking of all three levels is feasible for compatible references because y_3 is indirectly regulated through the two hydraulic couplings. The simulations use the common compatible reference $y_{1d} = y_{2d} = y_{3d} = 0.2$ m.

The outflow rate from Tank 2 is

$$q_{20} = z_2 S_p \sqrt{2g y_2}. \tag{4}$$

The control objective is to design $u_1(k)$ and $u_2(k)$ such that the liquid levels track the desired references, namely

$$\lim_{k\to\infty} y_i(k) = y_{id}(k), \quad i = 1,2,3, \tag{5}$$

in the presence of nonlinear dynamics, parametric uncertainty, external disturbances, and unknown leakage faults. The tracking error is defined by

$$e_i(k) = y_{id}(k) - y_i(k). \tag{6}$$

Using the forward Euler approximation, the derivative of the i-th tank level is represented as

$$\dot{y}_i(k) \approx \frac{y_i(k+1) - y_i(k)}{T_s}, \quad i = 1,2,3 \tag{7}$$

where T_s is the sampling time. Therefore, the discrete-time faulty model is expressed as

$$\begin{aligned} y_i(k+1) = {} & F_i(\cdot) + G_i(\cdot)\big[u_i(k) \\ & + \beta_i(k - T_i) f_i(k) + \chi_i(\cdot)\big], \quad i = 1,2,3. \end{aligned} \tag{8}$$

where $f_i(k)$ is the fault function, $\beta_i(k - T_i)$ is the corresponding fault time profile, and $\chi_i(\cdot)$ denotes the lumped uncertainty of the i-th subsystem.

2.3 Leakage fault profiles

For the abrupt leakage fault in Tank 1, the fault function and time profile are defined as

$$f_1(k) = -c_1 \pi V_1^2 \sqrt{2g y_1(k)}, \quad \beta_1(k - T_1) = U(k - T_1). \tag{9}$$

For the incipient leakage fault in Tank 2, the fault function and time profile are described by

$$\begin{aligned} f_2(k) &= -c_2 \pi V_2^2 \sqrt{2g y_2(k)}, \\ \beta_2(k - T_2) &= \left[1 - e^{-\alpha(k - T_2)}\right] U(k - T_2). \end{aligned} \tag{10}$$

where $U(\cdot)$ is the unit-step function, V_1 and V_2 are leakage-related coefficients, and T_1 and T_2 denote the occurrence times of the abrupt and incipient faults, respectively.

Scope with respect to other fault modes. Leakage faults were selected because they enter the hydraulic mass balance as unknown state-dependent outflows and provide both abrupt and incipient benchmark profiles. A pump loss-of-effectiveness fault can be represented by $u_{i,\mathrm{act}} = \rho_i u_i + \delta_i$ with $0 \leq \rho_i \leq 1$ and an additive bias δ_i; if its lumped effect is matched, bounded, and within the remaining pump authority, the same FBELC corrective channel can approximate it. A sensor fault instead corrupts the feedback $y_{i,m} = y_i + b_{i,s} + n_i$ and is generally unmatched; it requires a fault-detection/isolation module, redundant sensing, or an observer before the present controller. Complete pump outage cannot be guaranteed because the two-input plant loses control authority. These cases are therefore not claimed as validated here and are identified as experimental extensions [21].

3. Proposed FBELC fault-tolerant controller

3.1 Control decomposition and role of SMC-FBELC

The proposed controller is decomposed into two components. The nominal SMC term is responsible for driving the fault-free system to follow the desired liquid levels, whereas the FBELC-based corrective term compensates for the unknown fault dynamics and unmodeled uncertainties. This decomposition allows the controller to preserve the robustness of SMC while reducing the dependence on exact fault information through online FBELC learning.

The measured levels are fed back to form $e = y_d - y$. The nominal SMC generates u_N, whereas the FBELC uses the error-related signals and online learning law to generate u_C. Their sum is passed through the actuator saturation block before driving Pumps 1 and 2. Leakage faults and uncertainties enter the plant, and the three measured tank levels close the loop. This diagram distinguishes the FBELC internal structure in Fig. 2 from the complete closed-loop control architecture in Fig. 4.

The control input is therefore designed as

$$u_i(k) = u_{iN}(k) + u_{iC}(k), \quad i = 1,2. \tag{11}$$

where $u_{iN}(k)$ is the nominal SMC component and $u_{iC}(k)$ is the FBELC-based corrective component. For the nominal fault-free case, the SMC law is designed to enforce the desired tracking dynamics. A representative nominal control law can be written as

$$u_{iN}(k) = \frac{y_{id}(k+1) - y_i(k) + a T_s e_i(k) - T_s F_i(\cdot)}{T_s G_i(\cdot)}, \quad i = 1,2, \tag{12}$$

where $a > 0$ is a design constant. The corrective control $u_{iC}(k)$ is activated to compensate for the fault-induced term $\beta_i(k - T_i) f_i(k)$ and the uncertainty $\chi_i(\cdot)$.

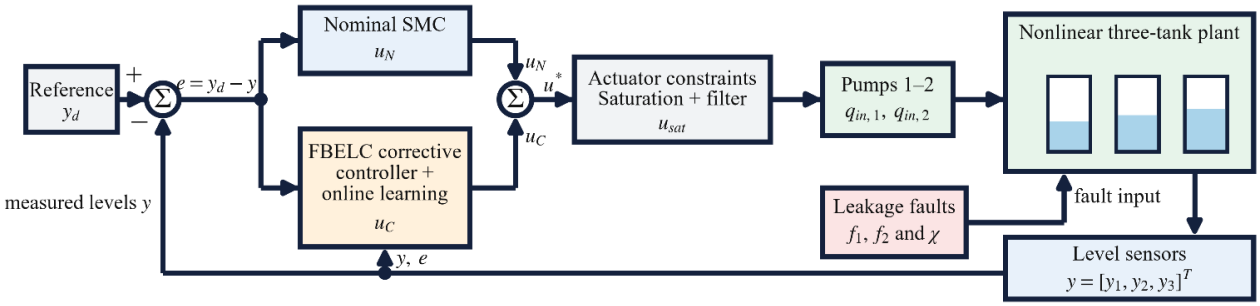


Figure 4. Overall closed-loop architecture of the proposed SMC–FBELC fault-tolerant control system.

For physical implementation, the computed demand $u_i^* = u_{iN} + u_{iC}$ is converted to the pump command using $u_{i,\mathrm{sat}} = \min\{u_{i,\max}, \max(0, u_i^*)\}$, followed by the discrete first-order command filter $u_i(k) = u_i(k-1) + \lambda_u[u_{i,\mathrm{sat}}(k) - u_i(k-1)]$, $0 < \lambda_u \le 1$. A rate limiter $|u_i(k) - u_i(k-1)| \le \Delta u_{i,\max}$ may be applied when pump specifications are available. The non-negativity constraint prevents an inflow pump from demanding reverse flow, saturation enforces rated capacity, and the filter/rate limiter suppress sharp changes. Anti-windup is implemented by updating the corrective learner with the applied rather than unconstrained command when saturation is active. The reported figures show volumetric flow demand in m^3/s; the apparently small numerical values result from SI units (1×10^{-3} $\mathrm{m}^3/\mathrm{s} = 1$ L/s). The narrow initial peak in Fig. 6(c) is caused by the step reference and should be interpreted as an unconstrained simulation demand, not as evidence that an ideal pump can change instantaneously. Accordingly, practical selection of $u_{i,\max}$, $\Delta u_{i,\max}$, and λ_u must use the pump data sheet, and feasibility requires sufficient authority to balance the nominal outlet and worst admissible leakage. This limitation is now stated explicitly rather than claiming direct hardware realization from the ideal-demand curve.

3.2 FBELC network structure

The FBELC network consists of the input space, sensory cortex space, amygdala weight space, orbitofrontal cortex weight space, and output space. Its architecture is shown in Fig. 2.

The input vector is defined as

$$I = [I_1, I_2, \ldots, I_n]^T \in \mathbb{R}^n. \tag{13}$$

The Gaussian membership function in the sensory cortex space is given by

$$S_{ij} = \exp\left[-\frac{(I_i - m_{ij})^2}{2s_{ij}^2}\right], \quad i = 1,2,\ldots,n,\ j = 1,2,\ldots,m. \tag{14}$$

where m_{ij} and s_{ij} are the mean and variance of the j-th block of the i-th input. The amygdala output is

$$a = \sum_{i=1}^{n}\sum_{j=1}^{m} S_{ij} v_{ij}. \tag{15}$$

The orbitofrontal cortex output is

$$o = \sum_{i=1}^{n}\sum_{j=1}^{m} S_{ij} w_{ij}. \tag{16}$$

Thus, the FBELC output is designed as

$$u_{\mathrm{FBELC}} = a - o = \sum_{i=1}^{n}\sum_{j=1}^{m} S_{ij}(v_{ij} - w_{ij}). \tag{17}$$

The parameter-adjustment signal is selected as

$$d_i = b_i \chi_i + c\, u_{\mathrm{FBELC}}, \quad i = 1,2,\ldots,n, \tag{18}$$

where b_i and c are positive gains. The updating laws for the amygdala and orbitofrontal weights are given by

$$\Delta v_{ij} = \alpha S_{ij} \max(0, d_i - a), \tag{19}$$

and

$$\Delta w_{ij} = \beta S_{ij}(u_{\mathrm{FBELC}} - d_i), \tag{20}$$

where $\alpha > 0$ and $\beta > 0$ are learning rates. The parameter-adjustment mechanism of FBELC is illustrated in Fig. 3.

Parameter-tuning guideline and sensitivity. All FBELC inputs are first normalized to comparable ranges. The gains $b_i > 0$ weight the uncertainty/error stimulus and $c > 0$ scales feedback of the FBELC output in d_i; they are selected first so that neither term dominates d_i over the intended operating domain. Next, α and β are increased gradually from 10^{-5} while monitoring RMSE, peak control flow, and weight oscillation. The adopted $\alpha = \beta = 10^{-4}$, $b = 0.9$, and $c = 1$ provide conservative per-sample adaptation: although 10^{-4} appears small, the update is executed at every sampling instant and accumulated over the full run. Larger learning rates accelerate the initial weight change but increase oscillation and sharp control corrections; smaller values give smoother commands but slower fault compensation. The Lyapunov result is not tied to these exact numerical values: it requires positive learning/adaptive gains, bounded normalized basis functions, and bounded/projected parameter estimates. Thus, moderate positive variations principally affect transient speed and ultimate-bound size rather than the sign of the Lyapunov decrease. In implementation, $\alpha, \beta \in [10^{-5}, 10^{-3}]$, $b \in [0.5, 1.2]$, and $c \in [0.5, 1.5]$ constitute practical search intervals; values outside them should be revalidated because excessive gains can excite noise/actuator dynamics, whereas near-zero gains can delay accommodation.

3.3 Corrective control design

Let the unknown lumped fault-induced dynamics and uncertainties be denoted by $\Delta(x,t)$, where x is the closed-loop state vector. Based on the universal approximation capability of the FBELC network, $\Delta(x,t)$ can be represented as

$$\Delta(x,t) = W^{*T}\Gamma(x) + J(x,t) \tag{21}$$

where W^* is the ideal constant weight matrix, $\Gamma(x)$ is the FBELC basis-function vector, and $J(x,t)$ is the bounded approximation error. The FBELC-based corrective controller is selected as

$$u_C = -\hat{W}^T\Gamma(x) - \hat{\tau}\,\mathrm{sgn}(\psi(x)), \tag{22}$$

where $\hat{W}$ is the online estimate of W^*, $\hat{\tau}$ is the online estimate of the uncertainty bound, and $\psi(x)$ is the Lyapunov-related filtered error vector. The adaptive laws are designed as

$$\dot{\hat{W}}_k = \xi_1 b_k \psi(x), \quad k = 1,2,\ldots,n_b, \tag{23}$$

and

$$\dot{\hat{\tau}} = \xi_2 \psi^T(x)\,\mathrm{sgn}(\psi(x)), \tag{24}$$

where $\xi_1 > 0$ and $\xi_2 > 0$ are adaptive gains, b_k is the k-th basis vector, and n_b is the number of basis functions.

4. Stability analysis

This section provides a clearer Lyapunov-based stability analysis for the proposed SMC-FBELC controller. The following assumptions are introduced to make the stability conclusion explicit.

Assumption 1. The nominal closed-loop system under the nominal SMC law admits a continuously differentiable Lyapunov function $V_N(x)$ satisfying

$$\alpha_1(\|x\|) \le V_N(x) \le \alpha_2(\|x\|), \tag{25}$$

and

$$\frac{\partial V_N}{\partial x}\left[F(x,t) + G(x,t)u_N\right] \le -\alpha(\|x\|), \tag{26}$$

where $\alpha_1(\cdot)$, $\alpha_2(\cdot)$, and $\alpha(\cdot)$ are positive functions.

Assumption 2. The lumped uncertainty and approximation error are bounded. Specifically, there exists an unknown positive constant τ^* such that

$$\|\eta(x,t) + J(x,t)\| \le \tau^*, \tag{27}$$

where $\eta(x,t)$ denotes the unmodeled uncertainty and $J(x,t)$ denotes the FBELC approximation error.

Assumption 3. The FBELC network can approximate the unknown nonlinear fault function over a compact operating domain. That is, there exists an ideal weight matrix W^* such that the approximation residual $J(x,t)$ remains bounded.

Define the estimation errors as

$$\tilde{W} = \hat{W} - W^*, \quad \tilde{\tau} = \hat{\tau} - \tau^*. \tag{28}$$

Consider the Lyapunov function candidate

$$V = V_N(x) + \frac{1}{2\xi_1}\mathrm{tr}(\tilde{W}^T\tilde{W}) + \frac{1}{2\xi_2}\tilde{\tau}^2. \tag{29}$$

Taking the time derivative of (29) gives

$$\dot{V} = \dot{V}_N + \frac{1}{\xi_1}\mathrm{tr}(\tilde{W}^T\dot{\hat{W}}) + \frac{1}{\xi_2}\tilde{\tau}\dot{\hat{\tau}}. \tag{30}$$

Substituting the closed-loop system into $\dot{V}_N$ yields

$$\begin{aligned}\dot{V} \le{}& -\alpha(\|x\|) + \psi^T(x)\big[u_C + \eta(x,t) \\ &+ W^{*T}\Gamma(x) + J(x,t)\big] \\ &+ \frac{1}{\xi_1}\mathrm{tr}(\tilde{W}^T\dot{\hat{W}}) + \frac{1}{\xi_2}\tilde{\tau}\dot{\hat{\tau}}.\end{aligned} \tag{31}$$

Using $W^{*T}\Gamma(x) = \hat{W}^T\Gamma(x) - \tilde{W}^T\Gamma(x)$ and substituting the corrective controller (22), one obtains

$$\begin{aligned}\dot{V} \le{}& -\alpha(\|x\|) + \psi^T(x)\big[-\tilde{W}^T\Gamma(x) \\ &+ \eta(x,t) + J(x,t) - \hat{\tau}\,\mathrm{sgn}(\psi(x))\big] \\ &+ \frac{1}{\xi_1}\mathrm{tr}(\tilde{W}^T\dot{\hat{W}}) + \frac{1}{\xi_2}\tilde{\tau}\dot{\hat{\tau}}.\end{aligned} \tag{32}$$

By applying the adaptive laws (23) and (24), the weight-estimation term $-\psi^T(x)\tilde{W}^T\Gamma(x)$ is cancelled by $(1/\xi_1)\mathrm{tr}(\tilde{W}^T\dot{\hat{W}})$. Therefore, the derivative becomes

$$\begin{aligned}\dot{V} \le{}& -\alpha(\|x\|) + \psi^T(x)\big[\eta(x,t) + J(x,t)\big] \\ &- \hat{\tau}\|\psi(x)\|_1 + \tilde{\tau}\|\psi(x)\|_1.\end{aligned} \tag{33}$$

Since $\tilde{\tau} = \hat{\tau} - \tau^*$, (33) can be rewritten as

$$\dot{V} \le -\alpha(\|x\|) + \psi^T(x)\big[\eta(x,t) + J(x,t)\big] - \tau^*\|\psi(x)\|_1. \tag{34}$$

Using Assumption 2, the following inequality is obtained:

$$\begin{aligned}\dot{V} \le{}& -\alpha(\|x\|) + \|\psi(x)\|_1\|\eta(x,t) + J(x,t)\| \\ &- \tau^*\|\psi(x)\|_1 \le -\alpha(\|x\|) \le 0.\end{aligned} \tag{35}$$

Thus, $V(t)$ is non-increasing and all closed-loop signals, including $x(t)$, $\tilde{W}(t)$, and $\tilde{\tau}(t)$, are bounded. Moreover, because $\dot{V} \le -\alpha(\|x\|)$, the tracking error is bounded and converges to a neighborhood of zero determined by the approximation capability of the FBELC network and the residual uncertainty bound. If the approximation error is negligible and the boundedness condition is exactly satisfied, asymptotic convergence can be achieved; otherwise, the closed-loop system is uniformly ultimately bounded.

5. Simulation results and discussion

5.1 Simulation setup

The simulation settings are summarized before presenting the four test cases. The initial liquid levels are selected as

$$y_1(0) = y_2(0) = y_3(0) = 0.15\,\mathrm{m} \tag{36}$$

The desired liquid levels are

$$y_{1d}(k) = y_{2d}(k) = y_{3d}(k) = 0.2\,\mathrm{m}. \tag{37}$$

The three-tank parameters are $A = 0.0154$ m^2, $S_p = 5 \times 10^{-5}$ m^2, $g = 9.8$ m/s^2, $z_1 = 1$, $z_2 = 0.8$, and $z_3 = 1$. The uncertainty values are selected as $\chi_1 = 3.5 \times 10^{-3}$, $\chi_2 = 2.5 \times 10^{-3}$, and $\chi_3 = 6.5 \times 10^{-3}$. The FBELC learning parameters are $\alpha = 0.0001$, $\beta = 0.0001$, $b = 0.9$, and $c = 1$. The simulation horizon is 1000 s. The fault occurrence times are selected as $T_1 = 270$ s or $T_1 = 273$ s for the abrupt leakage fault and $T_2 = 426$ s for the incipient leakage fault. For quantitative comparison, the RMSE is computed as

$$\mathrm{RMSE}_i = \sqrt{\frac{1}{N}\sum_{k=1}^{N} e_i^2(k)}, \quad i = 1,2,3. \tag{38}$$

where N is the total number of sampling points.

Figure units. In Figs. 5–8, every liquid-level y-axis is in metres (m), every tracking-error y-axis is in metres (m), and

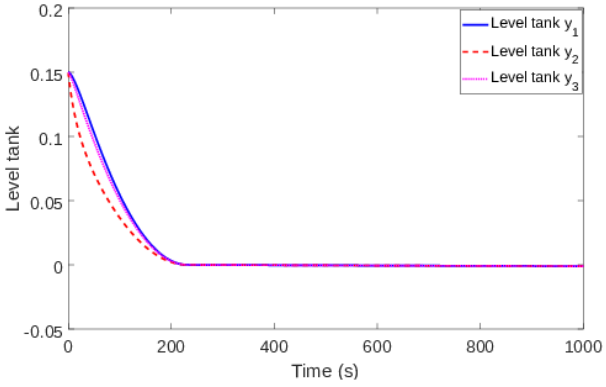


Figure 5. Three-tank system with no fault and no control. [Level: m; time: s]

every control-signal y-axis is volumetric flow rate in cubic metres per second (m^3/s). Time axes are in seconds (s). These units are also stated in the corresponding captions to remove ambiguity.

In (38), $e_1(k) = y_{1d}(k) - y_1(k)$, $e_2(k) = y_{2d}(k) - y_2(k)$, and $e_3(k) = y_{3d}(k) - y_3(k)$ are the level-tracking errors of Tanks 1, 2, and 3, respectively, at sample k; all have units of metres. RMSE_i is therefore the root mean square of the N samples of the i-th level error and also has units of metres. The 'Average RMSE' in Table 1 is the arithmetic mean $(\mathrm{RMSE}_1 + \mathrm{RMSE}_2 + \mathrm{RMSE}_3)/3$, not the RMSE of a pooled error vector.

5.2 Case 1: no fault and no control

In Case 1, the tank system is considered without leakage faults and without control inputs, namely $f_1(k) = 0$, $f_2(k) = 0$, $u_1(k) = 0$, and $u_2(k) = 0$. The response is shown in Fig. 5.

As shown in Fig. 5, the liquid levels naturally decrease because no control input is supplied to compensate for the outflow and inter-tank hydraulic interactions. This case provides a baseline illustrating that the uncontrolled tank system cannot maintain the desired liquid levels.

5.3 Case 2: no fault with nominal control

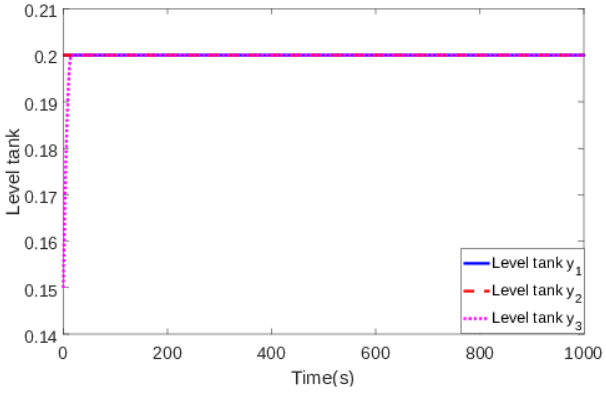
In Case 2, there is no leakage fault, i.e., $f_1(k) = 0$ and $f_2(k) = 0$, and the nominal control input $u_i(k) = u_{iN}(k)$ is applied for $i = 1, 2$. The simulation results are shown in Fig. 6.

Fig. 6 shows that the nominal SMC controller can drive the liquid levels to the desired value of 0.2 m when no leakage fault occurs. The tracking errors converge to a small neighborhood around zero, and the control signals remain bounded. This result confirms that the nominal control component is sufficient for the fault-free operating condition.

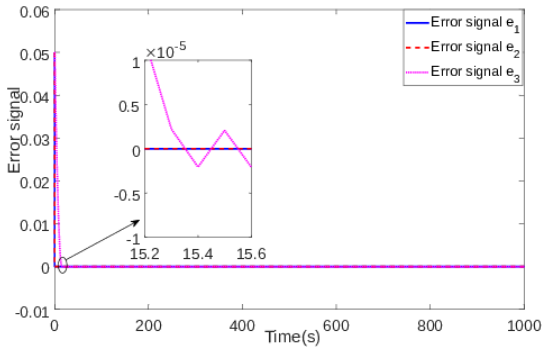
5.4 Case 3: abrupt leakage fault in Tank 1

In Case 3, an abrupt leakage fault is injected into Tank 1. The leakage dynamics are defined by (9), with $V_1 = 7.3 \times 10^{-2}$ and $T_1 = 273$ s. The control input is $u_i(k) = u_{iN}(k) + u_{iC}(k)$ for $i = 1, 2$. The simulation results are shown in Fig. 7.

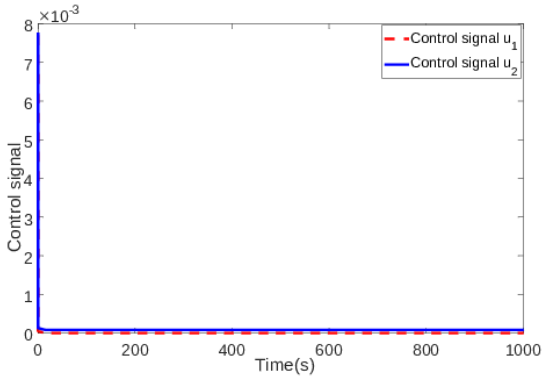
As shown in Fig. 7, the abrupt fault causes a transient deviation of the liquid level after the fault occurrence time. However, the FBELC corrective component rapidly compensates for the unknown leakage effect, and the tracking errors are driven back to a small neighborhood around zero.



(a) Tracking response. [Level: m; time: s]



(b) Error signal. [Error: m; time: s]



(c) Control signal. [Flow rate: m^3/s; time: s]

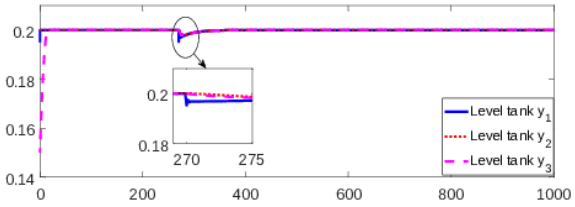
Figure 6. Three-tank system without fault under nominal control.

The bounded control signal also indicates that the proposed controller accommodates the abrupt fault without excessive control effort.

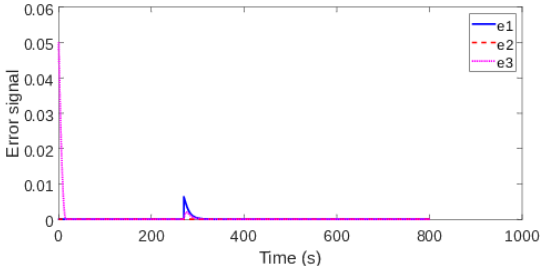
5.5 Case 4: abrupt fault in Tank 1 and incipient fault in Tank 2

In Case 4, an abrupt leakage fault is applied to Tank 1 and an incipient leakage fault is applied to Tank 2. The parameters are selected as $V_1 = 7.3 \times 10^{-2}$, $V_2 = 8.4 \times 10^{-2}$, $T_1 = 273$ s, $T_2 = 426$ s, and $\alpha = 0.063$. The simulation results are shown in Fig. 8.

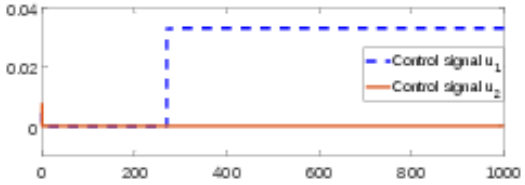
Fig. 8 demonstrates that the simultaneous occurrence of abrupt and incipient faults produces more severe transient tracking errors than the single-fault case. Nevertheless, the proposed SMC-FBELC controller compensates for both sudden and gradual fault effects. The tracking responses return to the desired liquid levels after transient deviations, confirming



(a) Tracking response. [Level: m; time: s]

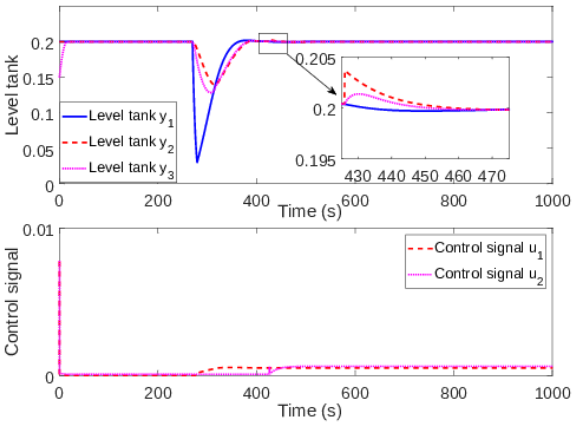


(b) Error signal. [Error: m; time: s]

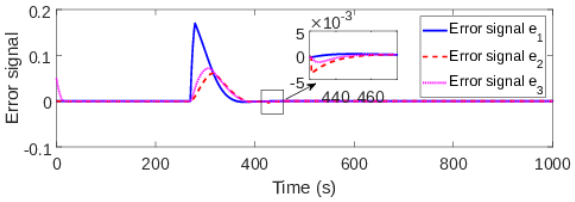


(c) Control signal. [Flow rate: m^3/s; time: s]

Figure 7. Three-tank system with abrupt fault in Tank 1.



(a) Tracking response (upper plot) and control signal (lower plot). [Level: m; flow rate: m^3/s; time: s]



(b) Error signal. [Error: m; time: s]

Figure 8. Three-tank system with fault 1 at $T_1 = 273$ s and fault 2 at $T_2 = 426$ s under the proposed method.

the fault-accommodation capability of the proposed method.

Table 1. The RMSE comparisons between proposed FBELC, CMAC, and FCMAC.

Method	$RMSE_1$	$RMSE_2$	$RMSE_3$	Average RMSE
CMAC [8]	0.0301	0.0212	0.0224	0.0246
FCMAC [16]	0.0269	0.0184	0.0179	0.0211
Proposed FBELC	0.0263	0.0121	0.0149	0.0178

5.6 Quantitative comparison

The RMSE comparison for Case 4 is listed in Table 1.

The proposed FBELC method achieves the lowest average RMSE of 0.0178, which is smaller than CMAC and FCMAC. Compared with CMAC, the average RMSE is reduced from 0.0246 to 0.0178, corresponding to an improvement of approximately 27.6%. Compared with FCMAC, the average RMSE is reduced from 0.0211 to 0.0178, corresponding to an improvement of approximately 15.6%. These results verify that the proposed SMC-FBELC scheme improves tracking accuracy and fault accommodation under simultaneous abrupt and incipient leakage faults.

Computational burden and real-time relevance. Let $M = n \times m$ denote the number of active Gaussian receptive blocks per output. Each FBELC update evaluates M memberships, forms two weighted sums (amygdala and orbitofrontal outputs), and updates two M-element weight arrays; hence its online time and memory complexity are $O(M)$ per sample. CMAC has $O(r)$ arithmetic for r active addresses but also requires a quantized address/memory table whose total storage grows with the allocated grid. FCMAC additionally evaluates fuzzy receptive fields and adapts consequent weights, with complexity $O(r)$ but more address and receptive-field bookkeeping. FBELC therefore does not guarantee fewer operations for every configuration, but it avoids the large preallocated multidimensional memory table of conventional CMAC and uses only two dense weight arrays plus membership parameters. This compact, deterministic per-sample workload is favorable for low-power controllers when M is kept small, inactive rules are skipped, Gaussian terms are lookup-table approximated, and worst-case execution time is verified against the sampling period. Hardware timing and memory measurements remain future experimental work; no unsupported real-time claim is made from simulation alone.

6. Conclusion

This paper proposed an SMC-FBELC fault-tolerant control scheme for nonlinear three-tank systems subject to abrupt and incipient leakage faults. The nominal SMC component was designed to maintain the desired tracking behavior under fault-free operation, while the FBELC corrective component was used to approximate and compensate for unknown fault-induced dynamics and lumped uncertainties online. A Lyapunov-based analysis was provided to prove boundedness of the closed-loop signals and to clarify the stability conclusion. Simulation studies under four operating scenarios demonstrated that the proposed method can maintain liquid-level tracking under no-fault, single-fault, and simultaneous-fault conditions. The RMSE comparison further showed that the proposed FBELC-based method outperforms CMAC and FCMAC in terms of average tracking accuracy. Future work will focus on real-time implementation, actuator saturation,

measurement noise, and experimental validation on physical tank systems.

References

[1] M. Blanke, M. Kinnaert, J. Lunze, M. Staroswiecki, and J. Schröder, *Diagnosis and Fault-Tolerant Control*. Springer, 2006.

[2] E. Khalastchi and M. Kalech, "On fault detection and diagnosis in robotic systems," *ACM Computing Surveys (CSUR)*, vol. 51, no. 1, pp. 1–24, 2018.

[3] D. H. Pham, T. T. Huynh, and C. M. Lin, "Fault-tolerant control for robotic systems using a wavelet type-2 fuzzy brain emotional learning controller and a TOPSIS-based self-organizing algorithm," *International Journal of Fuzzy Systems*, vol. 25, pp. 1727–1741, 2023. DOI: 10.1007/s40815-023-01516-y

[4] Y. Zhang, W. Zhu, and A. Rosendo, "QR code-based self-calibration for a fault-tolerant industrial robot arm," *IEEE Access*, vol. 7, pp. 73 349–73 356, 2019.

[5] J. Zhang, C. Yuan, P. Stegagno, H. He, and C. Wang, "Small fault detection of discrete-time nonlinear uncertain systems," *IEEE Transactions on Cybernetics*, vol. 51, no. 2, pp. 750–764, 2021. DOI: 10.1109/TCYB.2019.2945629

[6] J. Korbicz, K. Patan, and M. Witczak, "Fault-tolerant control: Analytical and soft computing solutions," in *Automatic Control, Robotics, and Information Processing*, P. Kulczycki, J. Korbicz, and J. Kacprzyk, Eds., Cham: Springer International Publishing, 2021, pp. 565–588.

[7] D. Zhu and M. Kong, "Adaptive fault-tolerant control of nonlinear systems: An improved CMAC-based fault learning approach," *International Journal of Control*, vol. 80, no. 10, pp. 1576–1594, 2007.

[8] C.-M. Lin, C.-C. Chung, Y.-J. Liu, and D. S. Yeung, "CMAC-based fault accommodation control for tank system," in *2010 International Conference on Machine Learning and Cybernetics*, vol. 6, 2010, pp. 2771–2776.

[9] Y. Sun and C.-M. Lin, "A hybrid PSO-parallel fuzzy brain emotional learning classifier for medical diseases diagnosis," *Journal of Intelligent Fuzzy Systems*, pp. 1–8, 2020.

[10] C. M. Lin, D. H. Pham, and T. T. Huynh, "Encryption and decryption of audio signal and image secure communications using chaotic system synchronization control by TSK fuzzy brain emotional learning controllers," *IEEE Transactions on Cybernetics*, pp. 1–15, 2021. DOI: 10.1109/TCYB.2021.3134245

[11] Z. Taifei and S. Shiyuan, "A fault-tolerant topology control algorithm for wireless ultraviolet light covert communication network in cluster UAV," *Photonic Network Communications*, vol. 42, no. 1, pp. 40–48, 2021. DOI: 10.1007/s11107-021-00936-w

[12] L.-Y. Hao, H. Zhang, T.-S. Li, B. Lin, and C. P. Chen, "Fault tolerant control for dynamic positioning of unmanned marine vehicles based on TS fuzzy model with unknown membership functions," *IEEE Transactions on Vehicular Technology*, vol. 70, no. 1, pp. 146–157, 2021.

[13] M. Ayyıldız and U. Tilki, "Fault tolerant control of wheeled mobile robots using adaptive sliding mode controller," in *2021 International Conference on INnovations in Intelligent SysTems and Applications (INISTA)*, 2021, pp. 1–6.

[14] T.-T. Huynh, C.-M. Lin, T.-L. Le, V.-P. Vu, and F. Chao, "Self-organizing double function-link fuzzy brain emotional control system design for uncertain nonlinear systems," *IEEE Transactions on Systems, Man, and Cybernetics: Systems*, 2020.

[15] L. Ma, Y. Huang, L. Zhou, J. Wang, and D. Shi, "Fault tolerant control for a class of nonlinear system with actuator faults," *Asian Journal of Control*, vol. 23, no. 1, pp. 474–485, 2021.

[16] F. Chao, D. Zhou, C.-M. Lin, C. Zhou, M. Shi, and D. Lin, "Fuzzy cerebellar model articulation controller network optimization via self-adaptive global best harmony search algorithm," *Soft Computing*, vol. 22, no. 10, pp. 3141–3153, 2018.

[17] C. Edwards and S. K. Spurgeon, *Sliding Mode Control: Theory and Applications*. London, U.K.: Taylor & Francis, 1998.

[18] Y. Shtessel, C. Edwards, L. Fridman, and A. Levant, *Sliding Mode Control and Observation*. New York, NY, USA: Birkhäuser, 2014. DOI: 10.1007/978-0-8176-4893-0

[19] M. M. Polycarpou, "Fault accommodation of a class of multivariable nonlinear dynamical systems using a learning approach," *IEEE Transactions on Automatic Control*, vol. 46, no. 5, pp. 736–742, 2001.

[20] J. Morén and C. Balkenius, "A computational model of emotional learning in the amygdala," in *From Animals to Animats 6: Proceedings of the 6th International Conference on the Simulation of Adaptive Behaviour*, Cambridge, MA, USA: MIT Press, 2000.

[21] X. Han, R. Rammal, M. He, Z. Li, M. Cabassud, and B. Dahhou, "Dynamic and sensor fault tolerant control for an intensified heat-exchanger/reactor," *European Journal of Control*, vol. 69, p. 100 736, 2023. DOI: 10.1016/j.ejcon.2022.100736

[22] T.-T. Huynh, C.-M. Lin, T.-L. Le, N. Q. K. Le, V.-P. Vu, and F. Chao, "Self-organizing double function-link fuzzy brain emotional control system design for uncertain nonlinear systems," *IEEE Transactions on Systems, Man, and Cybernetics: Systems*, vol. 52, no. 3, pp. 1852–1868, 2022. DOI: 10.1109/TSMC.2020.3036404

[23] M.-S. Phan, T.-C. Do, V.-Q. Truong, and T.-V.-A. Nguyen, "Comparative analysis of SMC-LMI and LQR controllers for double inverted pendulum," *Journal of Measurement, Control and Automation*, vol. 4, no. 3, pp. 1–7, 2023. DOI: 10.64032/mca.v4i3.184

[24] Q.-D. D. Nguyen, X.-M. Dinh, P.-L. Dang, T.-L. Pham, T.-T. Duong, and L. X. Le, "A hybrid motion planning framework for three-wheeled mobile robots based on improved A* and nonlinear model predictive control," *Journal of Measurement, Control and Automation*, vol. 30, no. 2, pp. 42–55, 2026. DOI: 10.64032/mca.v30i2.414